ORIGINAL RESEARCH

Effect of ionic liquid on graphene decorated with copper nanostructure dispersion towards silicon/graphene/copper composites with enhanced thermal, electrical and antimicrobial properties

Eduardo Daniel Solorzano-Ojeda[1] · Saúl Sánchez-Valdes[1] · Luis Francisco Ramos-deValle[1] ·
Rebeca Betancourt-Galindo[1] · Luciano da Silva[1] · Salvador Fernández-Tavizón[1] · José Francisco Hernández-Gámez[1] ·
Odilia Pérez-Camacho[1] · Eduardo Ramírez-Vargas[1] · Diana Morales-Acosta[1] · José Alberto Rodríguez-González[1] ·
José Javier Borjas-Ramos[1]

Abstract

Graphene decorated with cooper nanostructures were prepared with and without ionic liquid (IL) using different milling times. The obtained samples were characterized by Raman, X-ray diffraction (XRD) and transmission electron microscopy (TEM), to analyze the effect of the grinding time on the copper particles adhesion to the graphene sheets. Composites of silicon with two contents of G/Cu, at two weight ratios, nanostructures were prepared and the crosslinking characteristics were analyzed by a rubber process analyzer. The thermal conductivity, electrical resistivity and antimicrobial characteristics against *E. coli* and *S. aureus* for these silicon/G/Cu composites were determined. It was found that the use of IL enhances the G/Cu nanostructures dispersion into the silicon polymer matrix with a noticeable improvement in thermal conductivity of 1.12 W/mK for a 7 wt% of G/Cu, a volume electrical resistivity of 4.1×10^{10} Ω cm with 7 wt% of G/Cu nanoparticles and antimicrobial response of 4.21 ± 0.11 to *E. coli* and 5.33 ± 0.11 to *S. aureus* with 7% of G/Cu nanoparticles. It was determined that π–π interactions between graphene and aromatic molecule of IL may be influencing the observed improvement in G/Cu dispersion and final composite performance. The novelty of this work is the use of IL to improve the G/Cu NPs dispersion into the silicon polymer matrix. This silicon/G/Cu composite could be an option to prepare medical devices for electrotherapy or face protection against COVID-19 or other silicon-based devices for medical applications.

Graphic abstract
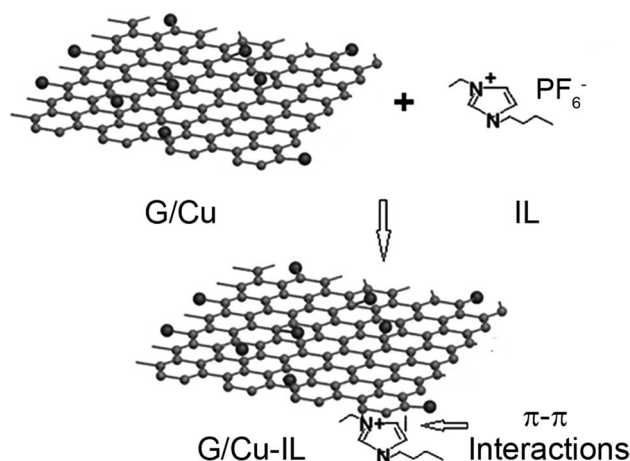
Extended author information available on the last page of the article

Introduction

Polydimethylsiloxane (PDMS), or silicon is commonly used for medical applications because of its stretchable and bending elastomeric characteristics [1, 2]. Some silicon devices for medical applications include stretchable electrodes or electrosurgical devices [3] in which the thermal and electrical conductivity together with antimicrobial properties are very important for their optimal performance. Silicon has been recently used for reusable respiratory masks and surgical masks respirators for protection against SARS-CoV-2 virus [4]. The continuous appearance of new threats to human health worldwide, such as new types of virus and the increasing number of antibiotic resistance bacteria, has conducted the research to a new antimicrobial strategy. Graphene can be considered as a single layer of two-dimensional carbon atoms with a sp2 bonding in a honeycomb lattice structure [5, 6]. It displays excellent mechanical properties, high electrical and thermal conductivity, biocompatibility and noticeable antibacterial activity [7–9]. Besides its antimicrobial properties, graphene has demonstrated an antiviral activity against other types of coronavirus such as porcine epidemic diarrhea virus, when it is used as component of a composite material [10]. On the other hand, copper nanoparticles (CuNPs) are recognized as one of the most efficient antimicrobial materials [11, 12]. It has been demonstrated the outstanding ability of CuNPs to inhibit the growth of fungi, bacteria and even many types of viruses [13, 14]. Even in the growing threat of the new SARS-CoV-2 virus, it has been reported the lower stability of this type of virus on the surface of metallic copper compared to plastic or stainless steel and other materials [15]. The reported antibacterial mechanism of each nanoparticle is different among them. But most of these mechanisms involve the destruction of bacterial membrane, creating an oxidative stress response, or the microorganism cell membrane damage through electrostatic interactions, which inhibit the synthesis of DNA or RNA, or reduce the enzymes production [16–18]. Graphene nanoparticles also have been recognized as antimicrobial agents because of its scissoring effect acting as s a sharp blade, which cause the bacteria membrane damage and irreversible electrolytes leakage from the bacteria cell [19, 20]. However, to achieve an optimal antibacterial activity of a polymer composite, the antibacterial nanoparticles must be perfectly dispersed and distributed into the polymer matrix. Because of the very small size of the nanoparticles, they have an inherent tendency to agglomerate which difficult the reaching of a final good dispersion. A good nanoparticle dispersion into the polymer matrix can be improved using ionic liquids. Ionic liquids (ILs) can be considered as semi-organic salts with good thermal and chemical stability, electrical conductivity, extremely low-vapor pressure, and nonflammable properties. ILs have been used to enhance the dispersion and stabilization of graphene and graphene oxide nanoparticles [21, 22]. Graphene nanosheets are a promising support material for metal nanoparticles to yield outstanding composites with high surface area, thermal and electrical properties as well as antimicrobial activity [23]. Decorating graphene nanosheets with copper nanoparticles incorporated into a silicon polymer matrix may produce nanocomposites with advanced antimicrobial characteristics [24]. Several reported works of composites using graphene doped with Cu nanoparticles have demonstrated that Cu nanospheres can be bonded to the G nanosheets surfaces by the charge-transfer interaction and physisorption [25–27]. This is because of the presence of some graphene imperfections such as polar hydroxyl or oxidized groups on the graphene surface [28]. In this work, graphene decorated with copper nanoparticles were dispersed into a silicon matrix using ionic liquid to obtain composites with enhanced thermal, electrical and antimicrobial characteristics. The novelty of this work is the noticeable improvement in G/Cu NPs dispersion into the silicon polymer matrix using IL. These composites represent a good option to prepare silicon-based devices for medical applications. Finally, to our knowledge, this is the first time that IL is used to improve the G/Cu NPs dispersion into silicon polymer matrix.

Experimental

Materials

Silicon elastomer Ecoflex 00-30 was obtained from Smooth-on, which was used as received. It consists of two components: a base prepolymer and a curing agent (in a 1:1 mix ratio). The graphene nanoparticles used in this study were from Cheap Tubes, Inc; with average particle thickness of 4 nm and lateral extension of 400–500 nm. The copper nanoparticles were from Nanostructured Amorphous Materials, Inc; with average particle diameter of 35 nm. 1-Hexyl-3-methylimidazolium hexafluorophosphate with molecular formula $C_{10}H_{19}F_6N_2P$ and molecular weight of 312.24, from Sigma-Aldrich was used as ionic liquid (IL). Finally, the ethylene glycol and methanol used were from J. T. Baker and Sigma-Aldrich, respectively.

Nanocomposite manufacturing

The preparation of graphene decorated with Cu NPs was carried out via high-energy mechanical mixing, in a SPEX 8000M Mixer/Mill. In a typical milling procedure, the stainless steel milling balls were introduced into the Teflon flask, along with 50 g of the graphene-copper mix, plus 2 mL of ethylene glycol and milled for the specific milling time of 3, 5 and 7 h. After this time, G–Cu NPs were washed with methanol to eliminate the excess of ethylene glycol. Then, the NPs were separated by centrifugation and dried at 80 °C for 24 h. The IL was incorporated into the dried G/Cu NPs using an agate mortar for 15 min of milling time until a homogeneous consistency was obtained. Silicon/G–Cu composites were prepared in an Xplore micro compounder at 25 °C and 100 rpm for 1 h. Samples with and without using IL were prepared. Two different graphene–copper ratios (70–30 and 50–50) of the copper-decorated graphene nanoparticles were each added to the silicon at two different concentrations; 3 and 7 wt%.

Characterization of composites

The XRD patterns of the products were obtained using a Siemens D-5000 using CuKα X-ray radiation. The surface morphologies and micro-structures of the composites were characterized by scanning and transmission electron microscopy using a Jeol-JSM-7401F with a STEM modulus and a field emission gun at an accelerating voltage of 200 kV. Particle size was obtained from the STEM images. This parameter was obtained considering at least 100 particles or their aggregates from an average of at least 10 observations. Rheological analysis of silicon/G–Cu nanocomposites was carried out in a Rubber Process Analyzer (RPA elite, from TA Instruments) at a deformation of 2°, a frequency of 1.667 Hz, and a temperature of 50 °C. Thermal conductivity of Nanocomposites was determined in a "Temperature Modulated Differential Scanning Calorimetry" (mDSC) [29], in accordance with ASTM-1952-11, using for each case two cylindrical samples of the same diameter (5.6 ± 0.1 mm), but of different heights (6.7 ± 0.1 and 2.0 ± 0.1 mm). The instrument used was a DSC Q200 from TA Instruments, using a Period of 30 s. Electrical resistivity (volumetric) was determined according to the four probe method using samples with $0.6 \times 10 \times 100$ mm^3.

The quantitative analysis of the antimicrobial activity for the prepared nanocomposites was determined against two types of bacteria that commonly colonize and infect a wound, a Gram-negative *E. coli* and a Gram-positive *S. aureus*. The assessment of antimicrobial activity was performed according to the JIS Z-2800:2001 now incorporated into the ISO standard 22196:2011 [30]. An initial inoculum of 50,000 CFU/mL (number of colony-forming units per milliliter, CFU/mL), was put in contact with nanocomposite samples. Also an inoculum without treatment as a positive control was used. This ISO standard establishes that the antimicrobial value shows the difference in the logarithmic value of viable cell counts between antimicrobial products and untreated products after the inoculation and incubation of bacteria. This value is calculated as follows:

$$R = \log \frac{B}{A} - \log \frac{C}{A} = \log \frac{B}{C} \qquad (1)$$

where R is the value of antimicrobial activity; A is the average number of viable bacterial cells immediately after inoculation on the untreated test piece; B is the average number of viable bacterial cells on the untreated test piece after 24 h; and C is the average number of viable bacterial cells on the antimicrobial test piece after 24 h. According to this standard, R value must not be less than 2 for an adequate antimicrobial efficacy and this value is equivalent to a 99% of antimicrobial efficiency.

Prior to the antimicrobial test, samples were washed with ethanol to remove any impurity from its surface and a corona discharge was applied using a Laboratory Corona Treater model BD-20 AC at a power of 10 kW for 1 min [31]. Antibacterial activity of silicon/G–Cu composite samples was also confirmed through determination of minimum inhibitory concentration (MIC), which is defined as the lowest concentration of antimicrobial agent at which no growth is observed in broth.

The antibacterial tests were performed using the disk diffusion method. Disk samples of selected concentrations of silicon/G–Cu composite samples [7 wt% G/Cu (50/50 and 70/30)] with and without IL were placed on agar plates that had previously been inoculated with both type of bacteria. The plates were incubated for 18 h at 37 °C. The antimicrobial activity of this sample was evaluated by observing the final inhibition zones (mm) that formed against both types of bacteria and also the minimum inhibitory concentrations (MICs) were determined as follows: Cultures containing various concentrations of silicon/G–Cu sample were prepared via dilution in phosphate-buffered saline (PBS). Dilutions were prepared at various silicon/G–Cu sample concentrations. An inoculum of both type of bacteria was prepared at 0.5 McFarland using a nephelometer (Becton, Dickinson and Company). Subsequently, 10 μL of each inoculum was transferred into a culture tube containing 11 mL of Mueller–Hinton broth. Afterward, 50 μL of each of these suspensions was placed in microplate wells for exposure to each of the sample dilutions. Once the designated incubation time had elapsed, the microplates were analyzed at 650 nm using an ELISA optical reader. The MICs were examined based on the optical density of each tube to determine the bacterial growth.

Results and discussion

Preparation and characterization of graphene doped with CuNPs

Graphene doped with CuNPs (G–Cu) samples were peppered by means of immobilization of Cu particles into graphene particles by shear stress during wet mixing. This method has been used elsewhere with good particle interactions [24, 25]. To determine the processing conditions to obtain G–Cu samples in the high-energy mill, three milling times were analyzed, 3, 5 and 7 h. The images obtained by TEM analysis of G–Cu NPs at 50/50 samples milled at these times can be seen in Fig. 1. Figure 1a shows the TEM image for the G–Cu sample at a milling time of 3 h in which noticeable G–Cu particle aggregates of more than 50 nm can be observed. This indicates that this milling time was not sufficient to generate the shear stress needed to disperse the particles and obtain a good distribution of Cu on the surface of graphene nanoplates [32]. Figure 1b shows the image obtained from the sample at 5 h of milling time. It can be seen a better nanoparticles dispersion with small particles and noticeable less aggregates with less of 50 nm sizes. A good distribution of Cu on the surface of graphene nanoplates can be observed. Also, in this figure the selected area electron diffraction (SAED) image obtained for these particles can be observed in which the main crystalline reflections of the monoclinic structure of CuNPs and CuO were indicated. The formation of copper oxide is expected since Cu is extremely sensitive to air. Figure 1c shows the sample obtained at a milling time of 7 h in which a similar morphology than sample at 5 h can be observed. From these results, the milling time of 5 h was selected for further analysis.

The crystalline structure of pristine graphene and CuNPs used and graphene doped with CuNPs (G–Cu NPs at 50/50) samples were characterized by X-ray diffraction (XRD) and the diffractogram image can be seen in Fig. 2.
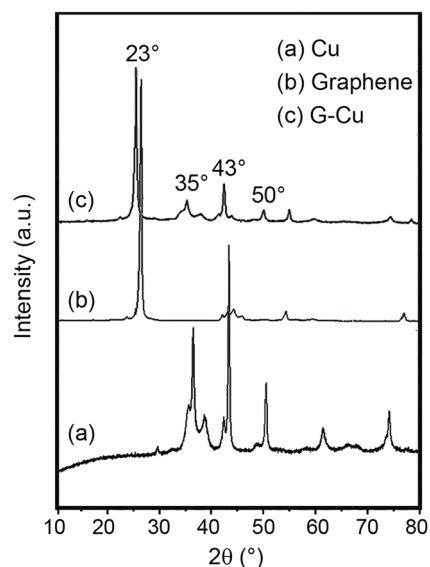

Fig. 2 XRD of nanoparticles: **a** Copper, **b** Graphene, **c** G–Cu NPs at 50/50 samples

In the copper spectrum, Fig. 2a, the characteristic diffraction peaks at 2Θ angles of 43°, 50° and 74°, which correspond to those expected in the metallic copper. Although a slight diffraction pattern corresponding to copper oxide was also found at 35°, which can be attributed to an oxide layer that could be formed on the surface of CuNPs. Since Cu is extremely sensitive to air, and the copper oxide phases are the most thermodynamically stable; therefore, the formation of an oxide layer on the surface of copper nanoparticles is inevitable [33]. In the graphene spectrum, Fig. 2b, the characteristic peak of this material could be found at a 2Θ diffraction angle of 25° which corresponds to the d_{002} reflection of graphene [34].

New small peaks are exhibited at 35°, 43° and 50° for the graphene doped with Cu (G–Cu NPs at 50/50) samples and as can be seen in Fig. 2c, the graphene characteristic peak at 25° is slightly shifted to lower diffraction
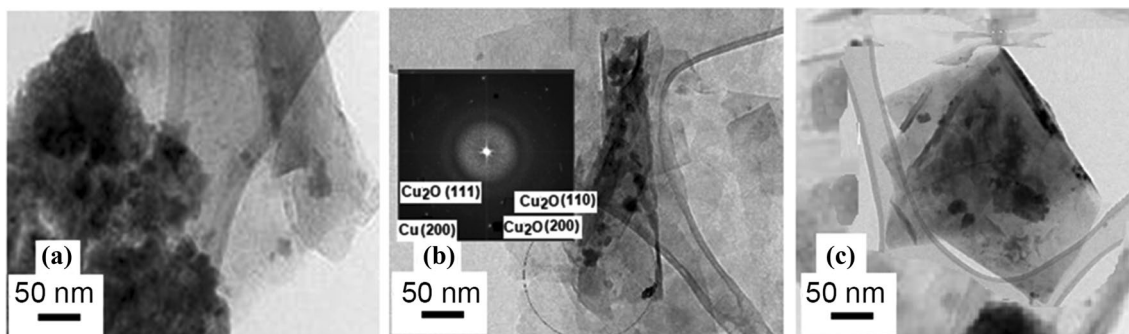

Fig. 1 TEM images of G–Cu NPs at 50/50 samples: **a** milled at 3 h, **b** milled at 5 h, and **c** milled at 7 h
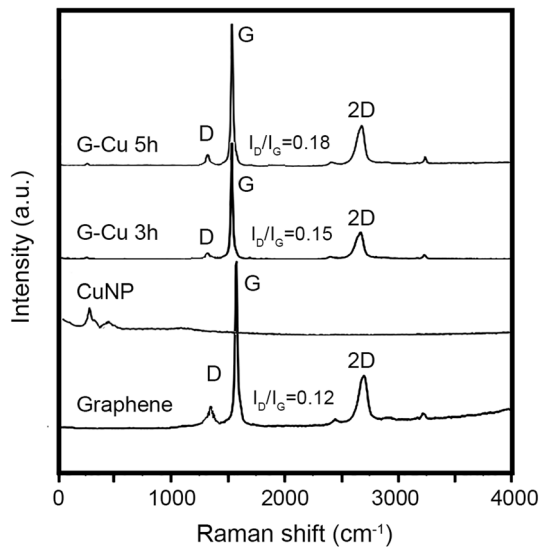
Fig. 3 Raman spectra of Graphene, Cu and G–Cu NPs at 50/50 samples milled at 3 and 5 h

angles and its intensity is slightly decreased due to the exfoliation of graphene layers and the presence of Cu in the graphene sheets [35].

Raman spectroscopy is the most used technique to analyze graphitic materials, especially in their structural characterization such as defects and order/disorder relationships. Figure 3 shows the Raman spectra of both graphene and Cu nanoparticles before the wet milling process and G–Cu NPs at 50/50 samples after 3 h and 5 h of milling. It can be seen the characteristic bands of each of the nanoparticles at 290 and 360 cm^{-1} for copper, and at 1350 cm^{-1} for the D band, 1580 cm^{-1} for the G band and 2700 cm^{-1} for the 2D band of graphene nanosheets. The D band is associated with structural defects, while the G band is associated with the stretching of the C–C bond from in-plane vibration of sp2 carbon atoms of graphitic materials. The parameter commonly used to refer to structural damage is the ratio of the intensity of the D band with respect to the intensity of the G band (ID/IG), it is considered that the higher its value, the greater the structural damage in the graphitic sample. As shown in this figure, the wet milling process generated an increase from 0.12 to 0.15 and 0.18 for 0, 3 and 5 h of mixing, respectively. Also, a slight shift of G and 2D peaks to lower Raman values can be observed. These observations indicate that some structural damage was induced by the shear applied during mixing. Also, this Raman shift suggests that Cu deposited on the graphene sheets could be introducing local doping, strain, and inhomogeneous charge distribution on the graphene sheets as was reported by other authors [36].

Silicon/G–Cu composites preparation

To analyze the crosslinking reaction process of silicon/G–Cu composites, various rheograms, shown in Fig. 4, were obtained at 50 °C. With this study it was possible to estimate the time necessary to mix the resin and the silicon crosslinking agent components to obtain the silicon crosslinked sample. The rheograms of the oscillatory rheometer shown in Fig. 4 compares the torque obtained at various crosslinking times for the pure silicon sample and the silicon composites with G–Cu at 3 and 7 wt% of G–Cu NPs at 50/50 G/Cu ratio. As can be seen, the crosslinking time at 50 °C goes from 10 min for the pure silicon sample to 9 and 7 min for the composite samples when adding 3 and 7 wt% of the hybrid nanoparticles. Also, an increase in torque was observed for composite samples. This decrease in crosslinking time and higher torque is due to the Cu NPs that, as some other metals, could be catalyzing the silicon crosslinking reaction [37]. This catalyzing effect of Cu NPs could promote greater chain crosslinking and, therefore, to an increase in torque.

Therefore, a mixing time of 9 min at room temperature was chosen to prepare the silicon/G–Cu composites. With these mixing conditions, there was enough time to disperse and distribute the nanoparticles into the silicon matrix with the guarantee that at these conditions, the silicon polymer is not yet crosslinked and the nanoparticles can be dispersed. Using these mixing conditions, samples of silicon with 3 and 7 wt% of G/Cu at 70/30 and 50/50 with and without using ionic liquid were prepared in the Xplore microcompounder.

Thermal conductivity

To determine thermal conductivity samples were prepared according to ASTM E 1952 standard. It can be observed in Fig. 5 that all the composite samples show higher thermal conductivity than pure silicon. Pure silicon sample shows a thermal conductivity of 0.2 W/[m K] which is in agreement
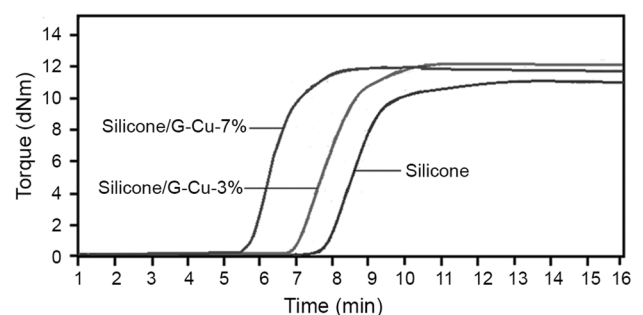

Fig. 4 Torque–time curves obtained in the RPA for samples of silicon and silicon/G–Cu composites at 3 and 7 wt% of G–Cu NPs at 50/50 G/Cu ratio
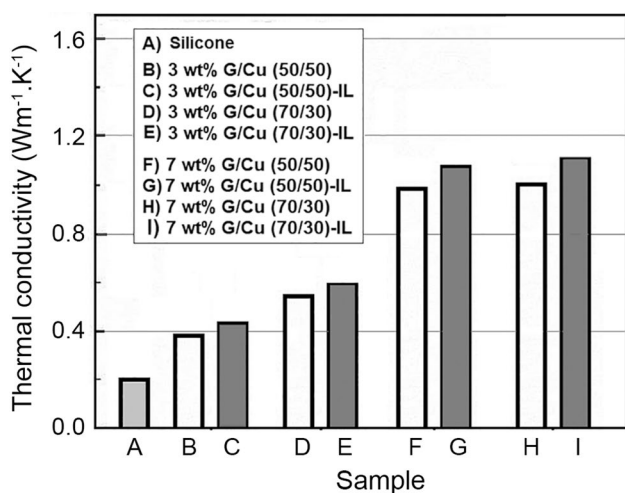
Fig. 5 Thermal conductivity of silicon and silicon/G–Cu composites

Fig. 6 Scheme of possible interactions between graphene and Copper and ionic liquid

to the values reported in the literature [38] for silicon materials (0.26 W/[m K]). It can be seen in this figure that the thermal conductivity is increased with the G–Cu NPs content which is related with the gradual formation of the thermally conductive network when the NP content increased from 3 to 7 wt%. The thermal conductivity of samples at 3 wt% of NPs shows different values between the nanoparticle ratios of 50/50 and 70/30. At this content, G–Cu NPs are dispersed randomly in the polymer matrix and are separated apart, not forming a percolated network. It can be said that at 3 wt% of nanoparticles, these conduction channels are not yet formed, so thermal conductivity already occurs through another mechanism. However, it can be seen that the thermal conductivity is slightly increased for samples in which IL was used which was attributed to the better dispersion induced by IL with the enchantment in conductivity. On the other hand, the thermal conductivity of the samples with a concentration of 7 wt% only a small difference between the thermal conductivity of both nanoparticles ratios was observed. Also, it can be seen that samples in which IL was used a slightly higher value of thermal conductivity were obtained. It could be explained that this content of nanoparticles is sufficient to form a thermal conductive bridge. And also, the better dispersion obtained of both nanoparticles into the polymer matrix using IL promotes the formation of a percolation network which is reflected in higher thermal conductivity. In this way, the thermal conductivity is not affected by the amount of copper deposited on the graphene surface. The difference between both particle ratios indicates that the thermal conductivity is affected by the greater amount of copper on the surface of graphene and by the dispersion promoted by the IL [39]. The values obtained can be explained according to the Nielsen's equation where the thermal conductivity of the compounds is insensitive to the intrinsic thermal conductivity of the nanoparticles when this
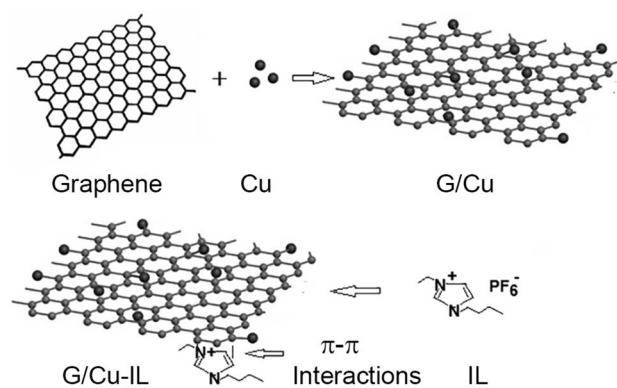
value is 100 times higher than the polymer matrix. Similar behavior was obtained by Yu et al. [40] who reported an increase of 4 times the value of the thermal conductivity of epoxy resin with graphene oxide. Another effect to be considered in our study system is the difference in shape and size of the two nanoparticles used in the system. Kemaloglu et al. [41] showed that silicon rubber compounded with larger boron nitrate particles exhibited higher thermal conductivity compared to smaller particles at constant filler loading. This behavior was attributed to the high packing density and ease of formation of conductive pathways. In our system, at a concentration of 7 wt% of G–Cu NPs, a thermal conductive bridge was formed which was enhanced by the particle dispersion induced by IL, with no significant difference between different graphene–copper compositions. The effect of IL in the dispersion of NPs can be summarized in Fig. 6 in which is schematized the possible π–π interactions between the cyclic groups of graphene and the IL [42].

Electric resistivity

Figure 7 shows the volume resistivity for silicon and silicon/G–Cu composites with and without using IL. All composite samples show lower volume resistivity than pure silicon. With increasing NPs content from 3 to 7 wt%, a sharp resistivity decreases was observed. Observing a noticeable difference in samples when using IL. It suggests that IL promotes a better particle dispersion with lower percolation thresholds. It is supposed that the better particle dispersion promoted by the IL formed a conductive network, which provides long charge transport path and increases the inter-particle contacts within the composite [43, 44]. Also, a noticeable reduction in volume resistivity was observed with G/Cu 70/30 ratios indicating that an increase of G NPs from 50 to 70 influences the conductive network and charge transport path.
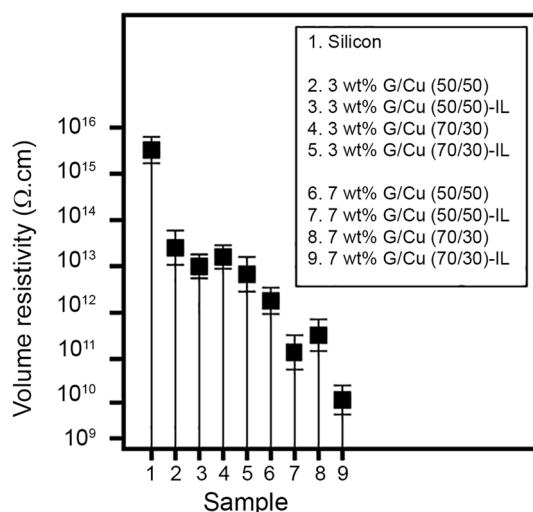
Fig. 7 Resistivity of silicon and silicon/G–Cu composite samples

Silicon/G–Cu composites morphology

Figure 8 shows the SEM images obtained for the Si:7%G/Cu(50/50) and Si:7%G/Cu(50/50)–IL composites. It can be clearly seen the effect in particles dispersion induced by the IL. Figure 8a shows noticeable G/Cu particle aggregates with very different sizes from 70 to 90 nm. On the other hand, sample with IL shows that the NPs are interspersed among the silicon particles to form a stable three-dimensional structure. It is noticeable a remarkable particle dispersion with Cu particles sizes around 20–30 nm which is the nominal size reported by the supplier of this type of particle. This indicates the IL improves the G/Cu NPs dispersion promoted by the π–π interactions between IL and G NPs. This obtained structure provides a better G/Cu NPs dispersion with a continuous transport channel for the electron transport, thereby imparting a good electrical conductivity and low electrical resistance to the entire composite. These π–π

interactions also have been reported by other authors such as Liu et al. [45] who demonstrated the enhanced lubricant properties of G/IL composite compared with G, IL or an IL + G mixture at the same mass fraction suggesting that the π–π interaction between G and IL promoted the synergistic lubricating effect in the composite. Also Gui et al. [46] have reported that graphene and phosphorus-containing ionic liquid ([PCMIM] PF6) were melt blended to obtain PLA nanocomposites with enhanced mechanical and flame retardant characteristics because of the strong interactions between G and IL.

Antimicrobial activity

Table 1 shows the antimicrobial activity against *E. coli* and *S. aureus* of silicon and composite samples. This table shows the *R* (antimicrobial activity) values obtained for silicon and each composite sample and the positive control of the bacteria inoculum without being in contact with any nanocomposite sample. As can be seen in this table, the lower antimicrobial activity (*R*) values were obtained in the positive control and silicon reference samples [43]. This suggests a remarkable growth of both types of bacteria in these samples. All the silicon/G–Cu composite samples showed higher antibacterial activity against the two types of evaluated microorganisms, compared with reference sample. This suggest that both types of nanoparticles are influencing the bacterial growth. It can be seen that higher NPs contents shows higher antimicrobial activity and a remarkably increase in antimicrobial activity was observed for samples in which IL was used. This was attributed to the better NP dispersion induced by the IL. The sample that exhibited the best antimicrobial activity was the composite with 7 wt% of G/Cu (50/50) using IL with an antimicrobial activity of 4.21 ± 0.11 for *E. coli* and 5.33 ± 0.11 for *S. aureus*. This difference between the antimicrobial activities for both types of bacteria can be attributed to the differences in the cell wall

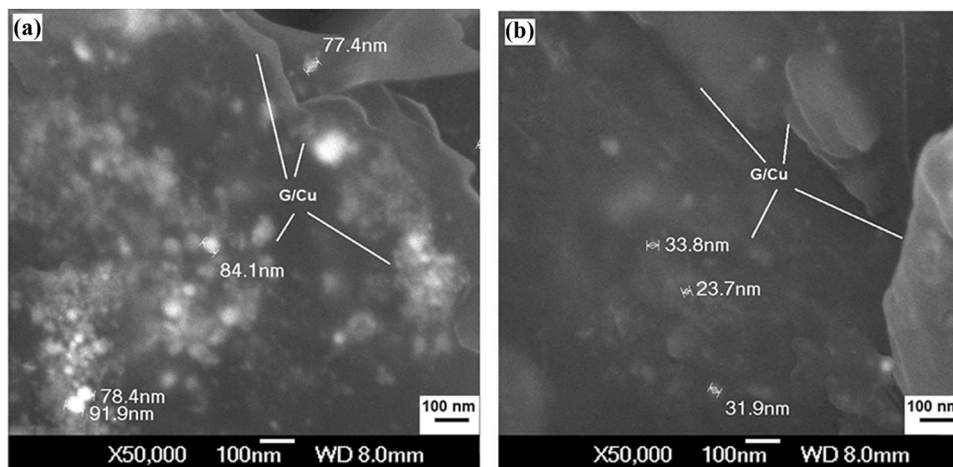**Fig. 8** SEM images of **a** Si:7%G/Cu(50/50) and **b** Si:7%G/Cu(50/50)–IL composites

Table 1 Antimicrobial results and minimum inhibitory concentration (MIC) against *E. coli* and *S. aureus* for positive control, silicon and composite samples

|	*E. coli* 25922		*S. aureus* 25923	
	R value	MIC (µg/ml)	*R* value	MIC (µg/ml)
Positive control	0.0	> 3000	0.0	> 3000
Silicon reference	0.02 ± 0.01	> 3000	0.02 ± 0.01	> 3000
Silicon/3 wt% G/Cu (50/50)	0.42 ± 0.07	–	0.63 ± 0.05	–
Silicon/3 wt% G/Cu (50/50)–IL	0.75 ± 0.09	–	0.94 ± 0.08	–
Silicon/3 wt% G/Cu (70/30)	0.91 ± 0.06	–	1.21 ± 0.07	–
Silicon/3 wt% G/Cu (70/30)–IL	1.36 ± 0.10	–	1.89 ± 0.09	–
Silicon/7 wt% G/Cu (50/50)	2.07 ± 0.09	375 ± 25	2.93 ± 0.10	255 ± 20
Silicon/7 wt% G/Cu (50/50)–IL	4.21 ± 0.11	275 ± 20	5.33 ± 0.11	148 ± 15
Silicon/7 wt% G/Cu (70/30)	2.82 ± 0.08	342 ± 18	3.12 ± 0.12	215 ± 21
Silicon/7 wt% G/Cu (70/30)–IL	3.85 ± 0.10	310 ± 11	4.01 ± 0.11	195 ± 19
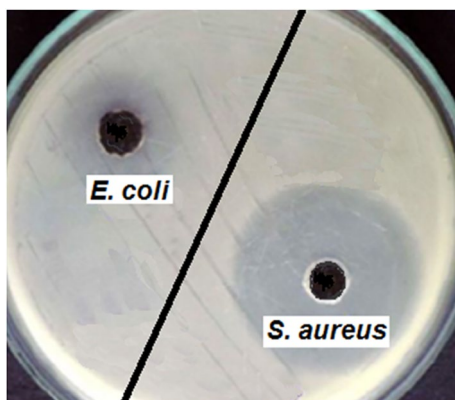
Fig. 9 Plate image of silicon/7 wt% G/Cu (50/50)–IL sample with *S. aureus* and *E. coli* bacteria

of Gram-positive and Gram-negative bacteria, their cellular physiology or even its metabolism [44, 47, 48]. Figure 9 shows an image of the silicon/7 wt% G/Cu (50/50)–IL sample in which IL was used and it can be observed a more notorious inhibition halo or inhibition zone for this sample against *S. aureus* which is in agreement with the antimicrobial activity (*R*) values obtained in Table 1. For instance, the Gram-negative bacteria (*E. coli*) have a peptidoglycan wall with an extra protective layer known as outer membrane, which hinders the penetration of any foreign particle through the cell membrane to inhibit its growth. This is in agreement with our results in which a higher antimicrobial activity was obtained for the Gram-positive bacteria of *S. aureus* [47]. The slightly better antimicrobial activity of samples with 50/50 than 70/30 of G/Cu suggest a better antimicrobial effect of Cu NPs than G nanosheets. According to the Japanese standard, the antimicrobial activity must have a value greater than 2 to be considered as antimicrobial material. It is reported that the ionic liquid increases the graphene dispersion; therefore, the G–Cu NPs are better dispersed into the silicon sample allowing a better antimicrobial

response. It is reported that the antimicrobial effect of Cu is based on the copper nanoparticles acting on the enzymes of the cell membrane of bacteria affecting their respiratory function [49, 50]. Thus, having a better dispersion of the G/Cu particles induced by the ionic liquid, a greater possibility of interaction of the particles with bacteria and this in turn would be reflected in a greater antimicrobial effect [42]. The obtained results indicated that the antibacterial activity of the silicon/G–CuNPs nanocomposite could arise from the combined effect of both types of NPs, the G sheets and the surface-deposited CuNPs. The literature reports a number of antibacterial mechanisms for Cu- and G-based materials, which include different modes of action such as cellular uptake, ion dissolution, or reaction oxide species (ROS) formation [50–53] for Cu and scissoring effect for G. Also the G NP size and distribution have been found to have an important influence on the antimicrobial activity. For instance Perreault et al. [54] demonstrated that GO-based surface coatings showed higher antimicrobial activity for smaller GO sheet sizes. The high antimicrobial activity of smaller GO sheets was found to be mediated through oxidative mechanisms due to the higher defect density introduced in GO sheets as size decreases. Also, Pham et al. [55] demonstrated the antimicrobial effect of G sheet edge length and angle orientation. They demonstrated that the density of the G edges was one of the principal parameters that contributed to the antibacterial behavior of the graphene nanosheets. This would promote the formation of pores in the bacterial cell wall, causing a subsequent osmotic imbalance and cell death.

Comparing the MIC results shown in Table 1, it can be observed that silicon composites with higher Cu content and in which IL was used, inhibited or stopped bacteria growth showing the higher antibacterial activity (higher *R* values) and lower MIC values. MIC values for silicon/7 wt% G/Cu (50/50)–IL sample were 275 ± 20 µg/ml against *E. coli* and 148 ± 15 µg/ml for *S. aureus*. These MIC values are in accordance to the reported values for CNT/Cu NPs by Cao

et al. [56]. According to these results, *S. aureus* was found to be more sensitive strain against silicon–G/Cu nanocomposites than *E. coli* which can be attributed to the lower thickness of the cell wall in the Gram-positive bacteria.

From these results, we can say that the best formulations to obtain enhanced thermal and electrical properties are those samples with higher graphene contents when using IL to enhance the filler dispersion (Silicon/7 wt% G/Cu (70/30)–IL). This indicates that the G has a notorious effect on the thermal and electrical conductivity, attributed to the trends to form a thermal and electrical conductive bridge by the well-dispersed G nanosheets. On the other hand, the best formulation to increase the antimicrobial properties is the samples with higher Cu NPs content (Silicon/7 wt% G/Cu (50/50)–IL). This suggests that Cu NPs have a strong antimicrobial effect attributed to their nanoparticle size and better dispersion that facilitates the continuous release of ions from their surface which are absorbed on the bacteria cell membrane due to electrostatic forces and inhibits its replication capability. This was confirmed by other authors [57] that attributed the antimicrobial mechanism of Cu and G NPs to the bacterial cell membrane disruption by the electrostatic interaction between the cationic charge of Cu and G NPs and the anionic charge of bacterial cellular components. These electrostatic connections increase the oxidative stress that damages bacterial protein as a consequence of cell membrane disruption.

Conclusions

Composites of silicon with graphene decorated with copper nanoparticles were obtained. The use of ionic liquid promoted a better NPs dispersion into the silicon matrix and enhanced the thermal, electrical and antimicrobial properties of the composites. It was concluded that the better dispersion of NPs promoted by the IL enhanced the thermal conductivity of silicon from 0.2 to 1.12 W/[m K], reduced the volume resistivity form 7×10^{15} to 4×10^{10} Ω cm and increased the antimicrobial activity against both types of bacteria, *S. aureus* and *E. coli*. It was concluded that the observed improvement in G/Cu dispersion and final composite performance was attributed to the π–π interactions between graphene and aromatic molecule of IL. It was possible to obtain a silicon composite with G/Cu NPs with enhanced thermal, electrical and antimicrobial properties that show their potentiality to be an option for medical devices for electrotherapy or face protection against COVID-19 or other silicon-based devices for medical applications.

References

1. Kaltenbrunner M, Sekitani T, Reeder J, Yokota T, Kuribara K, Tokuhara T, Drack M, Schwödiauer R, Graz I, Bauer-Gogonea S, Bauer S, Someya T (2013) An ultra-lightweight design for imperceptible plastic electronics. Nature 499:458–463
2. Eduok U, Faye O, Szpunar J (2017) Recent developments and applications of protective silicone coatings: a review of PDMS functional materials. Prog Org Coat 111:124
3. Maithani Y, Mehta BR, Singh JP (2021) Investigating the effect of silver nanorods embedded in polydimethylsiloxane matrix using nanoindentation and its use for flexible electronics. J Appl Polym Sci 138:50141
4. Manomaipiboon A, Pupipatpab S, Chomdee P, Chitsomkasem A, Apichatbutr Y, Boonyapatkul P, Trakarnvanich T (2020) The new silicone elastometric half-piece respirator, VJR-NMU: a novel and effective tool to prevent COVID-19. PLoS ONE 15(12):e0237206
5. Garino N, Zeng J, Castellino M, Sacco A, Risplendi F, Fiorentin MR, Bejtka K, Chiodoni A, Salomon D, Segura-Ruiz J, Pirri CF, Cicero G (2021) Facilely synthesized nitrogen-doped reduced graphene oxide functionalized with copper ions as electrocatalyst for oxygen reduction. 2D Mater Appl 5:2
6. Sánchez-Valdes S, Zapata-Domínguez AG, Martinez-Colunga JG, Mendez-Nonell J, Ramos de Valle LF, Espinoza-Martinez AB, Morales-Cepeda A, Lozano-Ramirez T, Lafleur PG, Ramirez-Vargas E (2018) Influence of functionalized polypropylene on polypropylene/graphene oxide nanocomposite properties. Polym Compos 39(4):1361
7. Broda J, Fabia J, Baczek M, Slusarczyk C (2020) Supramolecular structure of polypropylene fibers extruded with addition of functionalized reduced graphene oxide. Polymers 12(4):910
8. Balandin AA, Ghosh S, Bao W, Calizo I, Teweldebrhan D, Miao F, Lau CN (2008) Superior thermal conductivity of single-layer graphene. Nano Lett 8:902
9. Xie YY, Hu XH, Zhang YW, Wahid F, Chu LQ, Jia SR, Zhong C (2020) Development and antibacterial activities of bacterial cellulose/graphene oxide-CuO nanocomposite film. Carbohydr Polym 229:115456
10. Ye S, Shao K, Li Z, Guo N, Zuo Y, Li Q, Lu Z, Chen L, He Q, Han H (2015) Antiviral activity of graphene oxide: how sharp edged structure and charge matter. ACS Appl Mater Interfaces 7:21571
11. Ruparelia JP, Chatterjee AK, Duttagupta SP, Mukherji S (2008) Strain specificity in antimicrobial activity of silver and copper nanoparticles. Acta Biomater 4:707
12. Alayande AB, Obaid M, Kim IS (2020) Antimicrobial mechanism of reduced graphene oxide-copper oxide (rGO-CuO) nanocomposite films: the case of Pseudomonas aeruginosa PAO1. Mater Sci Eng C 109:110596
13. Ahmed MK, Afifi M, Uskokovic V (2020) Protecting healthcare workers during COVID-19 pandemic with nanotechnology: a protocol for a new device from Egypt. J Infect Public Health 13(9):1243
14. Chang Q, Xu W, Li N, Xue C, Wang Y, Li Y, Wang H, Yang J, Hu S (2020) Dynamic restructuring of carbon dots/copper oxide

supported on mesoporous hydroxyapatite brings exceptional catalytic activity in the reduction of 4-nitrophenol. Appl Catal B 263:118299

15. Doremalen N, Bushmaker T, Morris DH, Holbrook MG (2020) Aerosol and surface stability of SARS-CoV-2 as compared with SARS-CoV-1. N Engl J Med 382:3

16. Feng Y, Chang Y, Sun X, Liu N, Chang Y, Feng Y, Zhang H, Li X (2017) Understanding the property-activity relationships of polyhedral cuprous oxide nanocrystals in terms of reactive crystallographic facets. Toxicol Sci 156:480

17. Qian Y, Cui H, Shi R, Guo J, Wang B, Xu Y, Ding Y, Mao H, Yan F (2018) Antimicrobial anionic polymers: the effect of cations. Eur Polym J 107:181

18. Yang Z, Ma C, Wang W, Zhang M, Hao X, Chen S (2019) Fabrication of Cu2O-Ag nanocomposites with enhanced durability and bactericidal activity. J Colloid Interface Sci 557:156

19. Selim MS, Mo PJ, Hao Z, Fatthallah NA, Chen X (2020) Blade-like structure of graphene oxide sheets decorated with cuprous oxide and silicon carbide nanocomposites as bactericidal materials. J Colloid Interface Sci 578:698

20. Zheng H, Ma R, Gao M, Tian X, Li YQ, Zeng L, Li R (2018) Antibacterial applications of graphene oxides: structure-activity relationships, molecular initiating events and biosafety. Sci Bull 63:133

21. Abbaszadegan A, Gholami A, Abbaszadegan S, Aleyasin ZG, Ghahramani Y, Dorostkar S, Sharghi H (2017) The effects of different ionic liquid coatings and the length of alkyl chain on antimicrobial and cytotoxic properties of silver nanoparticles. Iran Endod J 12:481

22. Chinnappan A, Appiah-Ntiamoah R, Chung WJ, Kim H (2016) Ionic liquid functionalized graphene oxide decorated with copper oxide nanostructures towards H2 generation from sodium borohydride. Int J Hydrogen Energy 41(33):14491

23. Samak NA, Selim MS, Hao Z, Xing J (2020) Controlled-synthesis of alumina-graphene oxide nanocomposite coupled with DNA/sulfide fluorophore for eco-friendly "Turn off/on" H2S nanobiosensor. Talanta 211:120655

24. Selim MS, El-Safty SA, Fatthallah NA, Shenashen MA (2018) Silicone/graphene oxide sheet-alumina nanorod ternary composite for superhydrophobic antifouling coating. Prog Org Coat 121:160

25. Pullicino E, Zou W, Gresil M, Soutis C (2017) The effect of shear mixing speed and time on the mechanical properties of GNP/epoxy composites. Appl Comp Mats 24:301

26. Young M, Santra S (2014) Copper (Cu)–silica nanocomposite containing valence-engineered Cu: a new strategy for improving the antimicrobial efficacy of Cu biocides. J Agric Food Chem 62:6043

27. Kumar S, Ojha AK, Bhorolua D, Das J, Kumar A, Hazarika A (2019) Facile synthesis of CuO nanowires and Cu2O nanospheres grown on rGO surface and exploiting its photocatalytic, antibacterial and supercapacitive properties. Phys B: Cond Matter 558:74

28. Tian J, Wu S, Yin X, Wu W (2019) Novel preparation of hydrophilic graphene/graphene oxide nanosheets for supercapacitor electrode. Appl Surf Sci 496:143696

29. Hu M, Yu D, Wei J (2007) Thermal conductivity determination of small polymer samples by differential scanning calorimetry. Polym Test 26:333

30. International Organization for Standardization ISO (2011) Measurement of antibacterial activity on plastics and other non-porous surfaces (Standard No. 22196). Retrieved from, https://www.iso.org/standard/54431.html

31. Ghorbani HR, Molaei M (2017) Antibacterial nanocomposite preparation of polypropylene-Silver using Corona discharge. Prog Org Coat 112:187

32. Dong Z, Peng Y, Zhang X, Xiong D-B (2021) Plasma assisted milling treatment for improving mechanical and electrical properties of in-situ grown graphene/copper composites. Compos Commun 24:100619

33. Jeong S, Woo K, Kim D, Lim S, Kim JS, Shin H, Xia Y, Moon J (2008) Controlling the thickness of the surface oxide layer on Cu nanoparticles for the fabrication of conductive structures by ink-jet printing. Adv Funct Mater 18(5):679

34. Gong JR (2011) Graphene. Synthesis, characterization, properties and applications. September. eBook (PDF) ISBN: 978-953-51-5593-5

35. Hussain S, Akbar K, Vikraman D, Choi DC, Kim SJ, An KS, Jung S, Jung J (2015) Highly sensitive enzymeless glucose sensor based on 3D graphene-Cu hybrid electrodes. N Chem 9:7481–7487

36. Lee HJ, Novoselov KS, Shin HS (2010) Interaction between metal and graphene: dependence on the layer number of graphene. ACS Nano 5:608

37. Nakajima Y, Shimada S (2015) Hydrosilylation reaction of olefins: recent advances and perspectives. RSC Adv 5(26):20603

38. Wu S, Xiong Q, Li X, Chen D, Liu B (2020) Properties of thermally conductive silicone rubbers filled with admicellar polymerized polypyrrole-coated Al2O3 particles. J Appl Polym Sci 138:e50205

39. Huang C, Qian X, Yang R (2017) Influence of nanoparticle size distribution on thermal conductivity of particulate nanocomposites. EPL 117:24001

40. Yu A, Ramesh P, Sun X, Bekyarova E, Itkis ME, Haddon RC (2008) Enhanced thermal conductivity in a hybrid graphite nanoplatelet—carbon nanotube filler for epoxy composites. Adv Mater 20(24):4740

41. Kemaloglu S, Ozkoc G, Aytac A (2010) Properties of thermally conductive micro and nano size boron nitride reinforced silicon rubber composites. Thermochim Acta 499(1–2):40

42. Espinoza-Ibarra PA, Sánchez-Valdes S, Yáñez-Flores IG, Graciano-Verdugo AZ, Espinoza-Ibarra DF, Fernandez-Tavizon S, Ledezma-Pérez AS, Espinoza-Martínez AB, Rodríguez-Fernández OS, Betancourt-Galindo R, Ortega-Ortiz H, Ramirez-Vargas RR, Rodriguez-Gonzalez JA (2019) Preparation and characterization of cotton fibers coated with AA-IA hydrogel containing silver/graphene or graphene oxide nanoparticles. Polym Plast Tech Eng 58(7):753

43. Zhao S, Zhao H, Li G, Dai K, Zheng G, Liu C, Shen C (2014) Synergistic effect of carbon fibers on the conductive properties of a segregated carbon black/polypropylene composite. Mater Lett 129:72

44. Wang P, Deng G, Zhu H, Yin J, Xiong X, Zhang H (2021) Effect of pyrolytic carbon interface thickness on conductivity and tribological properties of copper foam/carbon composite. Appl Compos Mater 28:19

45. Liu L, Zhou M, Mo Y, Bai P, Wei Q, Jin L, You S, Wang M, Li L, Chen X, Li X, Tian Y (2021) Synergistic lubricating effect of graphene/ionic liquid composite material used as an additive. Friction 9(6):1568–1579

46. Gui H, Xu P, Hu Y, Wang J, Yang X, Bahader A, Ding Y (2015) Synergistic effect of graphene and an ionic liquid containing phosphonium on the thermal stability and flame retardancy of polylactide. RSC Adv 5(35):27814–27822

47. Ramirez-Barron SN, Sanchez-Valdes S, Betancourt R, Gallardo CA, Puente-Urbina B, Rodriguez-Fernandez OS, Carneiro-da Cunha MG, dos Santos- Correia MT, Sanchez-Martínez ZV (2021) Preparation and characterization of gelatin-gallic acid/ZnO nanocomposite with antibacterial properties as a promising multi-functional bioadhesive for wound dressing applications. Int J Adhes Adhes 104:102749

48. Avila-Alfaro JA, Sanchez-Valdes S, Ramos-deValle LF, Ortega-Ortiz H, Méndez-Nonell J, Patiño-Soto AP, Narro-Cespedes RI, Perera-Mercado YA, Avalos-Belmontes F (2013) Ultrasound

irradiation coating of silver nanoparticle on ABS sheet surface. J Inorg Organomet Polym Mater 23(3):673

49. Thurman RB, Gerba CP, Bitton G (1989) The molecular mechanisms of copper and silver ion disinfection of bacteria and viruses. Environ Control 184(4):295

50. Rajapaksha P, Cheeseman S, Hombsch S, Murdoch BJ, Gangadoo S, Blanch EW, Truong Y, Cozzolino D, McConville CF, Crawford RJ, Truong VK, Elbourne A, Chapman J (2019) Antibacterial properties of graphene oxide-copper oxide nanoparticle nanocomposites. ACS Appl Bio Mater 2(12):5687

51. Elbourne A, Truong VK, Cheeseman S, Rajapaksha P, Gangadoo S, Chapman J, Crawford RJ (2019) Methods in microbiology book series. Academic Press, Cambridge

52. Meghana S, Kabra P, Chakraborty S, Padmavathy N (2015) Understanding the pathway of antibacterial activity of copper oxide nanoparticles. RSC Adv 5(16):12293

53. Chatterjee AK, Chakraborty R, Basu T (2014) Mechanism of antibacterial activity of copper nanoparticles. Nanotechnology 25(13):135101

54. Perreault F, de Faria FA, Nejati S, Elimelech M (2015) Antimicrobial properties of graphene oxide nanosheets: why size matters. ACS Nano 9(7):7226–7236

55. Pham VTH, Truong VK, Quinn MDJ, Notley SM, Guo Y, Baulin VA, Kobaisi MA, Crawford RJ, Ivanova EP (2015) Graphene induces formation of pores that kill spherical and rod-shaped bacteria. ACS Nano 9(8):8458–8467

56. Cao Y, Javadhesari SM, Mohammadnejad S, Khodadustan E, Raise A, Akbarpour MR (2021) Microstructural characterization and antibacterial activity of carbon nanotube decorated with Cu nanoparticles synthesized by a novel solvothermal method. Ceramics Int. https://doi.org/10.1016/j.ceramint.2021.05.299

57. Singh A, Ahmed A, Keshri AK, Arora N, Anjum F, Rawat SS, Prasad A (2021) Membrane disruption potential of doped cuprous oxide nanoparticles against blaNDM-1 and mcr-1 positive colistin resistant *E. coli*. BioNanoScience 11:637–642

Authors and Affiliations

Eduardo Daniel Solorzano-Ojeda[1] · Saúl Sánchez-Valdes[1] · Luis Francisco Ramos-deValle[1] · Rebeca Betancourt-Galindo[1] · Luciano da Silva[1] · Salvador Fernández-Tavizón[1] · José Francisco Hernández-Gámez[1] · Odilia Pérez-Camacho[1] · Eduardo Ramírez-Vargas[1] · Diana Morales-Acosta[1] · José Alberto Rodríguez-González[1] · José Javier Borjas-Ramos[1]

✉ Saúl Sánchez-Valdes
saul.sanchez@ciqa.edu.mx

✉ Luis Francisco Ramos-deValle
luis.ramos@ciqa.edu.mx

1　Centro de Investigación en Química Aplicada, 25294 Saltillo, Coahuila, Mexico